Published in Design, Test, Integration, and Packaging of MEMS/MOEMS (DTIP2001), Cote d'Azur, France, April 2001

Dynamic Simulation of Optical MEM Switches

Timothy P. Kurzweg[a], Jose A. Martinez[a], Steven P. Levitan[a],
Philippe J. Marchand[b], and Donald M. Chiarulli[c]

[a]Department of Electrical Engineering, University of Pittsburgh
[b]Optical Micro Machines, San Diego, CA 92121
[c]Department of Computer Science, University of Pittsburgh

ABSTRACT

Micro-optical-electrical-mechanical systems (MOEMS) present a new set of challenges for systems on a chip (SoC) and mixed-technology designers including the need for mixed-signal multi-domain simulation. We present new modeling techniques for optical and mechanical MEM components and apply these models to the simulations of a MOEMS switch for optical fiber telecommunications applications.

Keywords: MOEMS, MEM, Mixed-Technology CAD, modeling, system-level simulation

1. INTRODUCTION

New fabrication techniques permit micro-electro-mechanical systems (MEMS) to use the same fabrication process as CMOS integrated circuits. In fact, they can be designed using many of the standard CAD lay-out packages. Analysis and even synthesis of both electrical and mechanical components have been the topic of recent research. However, one deficiency in the MEMS design process is the need for a system level simulation tool that crosses the domains of electronic, mechanical, and optical micro-systems. In order for a system simulation tool to be useful, it must be capable of modeling not only "first order" but also second order effects in each of the domains. In a practical sense, this means that for the electrical domain, we must model both digital and analog components, for the mechanical domain we need to capture both linear and non-linear stress/strain relationships, and for the optical domain we must support diffractive (scalar) models of optical propagation.

One application area where the need for this level of modeling and simulation is apparent is in the design of all-optical cross-connect switches for fiber based telecommunications networks. All-optical switches are becoming increasingly popular due to the many advantages that they possess over typical fiber optic switches. No longer is a costly conversion between the optical and electrical domain needed to switch data signals, as all-optical switches also reduce the insertion loss and crosstalk found in conventional fiber switches. The switching is achieved through the mechanical movement of mirrors steering the data path to the desired output. With the advancement of MEMS technology, these switches have become a reality, as the switches are small, fast, reliable, and eventually, will be inexpensive to produce.

In earlier work, we introduced our opto-electro-mechanical CAD tool, Chatoyant [1]. In this paper, we expand this work with new modeling techniques for greater accuracy in the simulation of micro-opto-electro-mechanical (MOEM) systems. We first discuss the modeling of second order component models, such as the modeling of the surface roughness and inherent curvature for micro-mirrors. We also expand our mechanical modeling techniques by including stress induced cantilever beams. Using these newer components, we simulate optical MEM systems with more accuracy. We conclude with a summary and a plan for future work.

2. OPTICAL MODELS

For CAD tools to be useful in the design of real systems, non-ideal components must be accurately modeled, such that the designer can simulate realistic system-level effects, caused by imperfections in the fabrication of these components. In this section, we first discuss the importance of understanding the accuracy versus computation time trade-off, which is always

Correspondence: S.P. Levitan. Other author information: T.P.K.; tim@ee.pitt.edu; Telephone: 412-624-0558; Fax: 412-624-8003. J.A.M.; jmarti@ee.pitt.edu; Telephone: 412-624-0558; Fax: 412-624-8003. S.P.L; steve@ee.pitt.edu; Telephone: 412-648-9663; Fax: 412-624-8003. P.J.M.; marchand@omminc.com; Telephone: 858-320-7164; Fax: 858-457-6853. D.M.C.; don@cs.pitt.edu; Telephone: 412-624-8839; Fax: 412-624-5249.

relevant in CAD simulation. We illustrate this trade-off with a discussion of our integration method that is used in our free-space light propagation model. We then introduce our model extensions for non-ideal components, which have high order effects, such as surface roughness, that introduces scattering, and the inherent curvature of micro-mirror devices.

1. Accuracy and Error

We have determined that the Rayleigh-Sommerfeld method is appropriate for system level optical propagation models for mixed-signal micro systems [2]. We use a 2-dimensional application of the Gaussian Quadrature technique in order to perform the integration in the Rayleigh-Sommerfeld equation. It is well known that Quadrature integration techniques offer the optimum estimate of the exact integration solution for the chosen number of points [3]. However, the accuracy of this method is dependent of the smoothness of the integrated function, since the function is effectively interpolated by a polynomial of degree 2N+1. In the Rayleigh-Sommerfeld expression, the possible causes of high order (i.e., "non-smooth") effects are found at the interactions of the complex wave function at the finite boundaries of the apertures. The Gaussian Quadrature method will result in an accurate solution if the discontinuities in the wave function at the boundaries are negligible. This condition is satisfied by the Rayleigh-Sommerfeld initial assumption that the aperture size is larger that the wavelength of the light.

The Gaussian Quadrature technique partitions the surface of integration into a grid or mesh. Each mesh point has an associated position and weight, which is used in the calculation of the integral. At the edges of the surface of integration, the mesh spacing is fine, and it becomes coarser towards the center. Therefore, the grid spacing is not equal, but is symmetric on all sides of the square integration plane.

For system level modeling, we are concerned about both the accuracy and computation speed of our simulations. The number of mesh, or grid, points in the Gaussian Quadrature integration method used for the Rayleigh-Sommerfeld formulation directly effects both accuracy and computation speed. As an example of the trade-off between computation speed and accuracy of a simulation result, we present the simulation of a plane wave (unity intensity) propagating to and reflecting off of a 10x10 μm square mirror. This reflected light is then propagated 10 μm to a 30x30 μm detection plane. With these small component sizes and propagation distances, this example requires the Rayleigh-Sommerfeld technique rather than a far-field or even a near-field approximation [2]. The following table shows results from multiple simulations, each with a different number of mesh points (24x24, 48x48, 96x96, 192x192, 348x348) used in the Gaussian Quadrature integration technique.

Gaussian Quadrauture Points	Avg. Mesh Size in nm (mirror)	λ/Avg_ Mesh (mirror)	Small mesh spacing in nm (det)	Largest mesh spacing in nm (det)	Avg. Mesh Size in nm (det)	λ/ Avg_ Mesh (det)	Power (at detector)	Comp. Time (sec)*	% Error
24 x 24 points	416.7	2.04	306.88	1922.0	1250	0.68	6.6321e-11	1.4	22.62
48 x 48 points	208.3	4.08	78.61	971.4	625	1.36	8.5229e-11	21.8	0.55
96 x 96 points	104.2	8.16	19.88	488.3	312.5	2.72	8.5675e-11	350.2	0.03
192 x 192 points	52.1	16.31	4.10	244.8	156.25	5.44	8.5698e-11	1487.0	0.01
384 x 348 points	26.0	32.7	1.25	122.6	78.125	10.90	8.5703e-11	~97200	0.00

* Dual Processor (Pentium III, 500 MHz), 1G RAM, Running Red Hat Linux 7.0

The output, in terms of intensity waveforms and contours, are given in Figure 1. As expected with such a small propagation distance, the intensity distribution shadows the size of the mirror, that is the small square shape with peaks at the corners of the aperture. At larger propagation distances (i.e., far field), the intensity contour would appear more typical of a square aperture, with a Gaussian shaped center and lobes on the x and y axes.

For this simulation, we consider the 348x348 point case as a "base case", and use it for comparison with the other results. The simulation computation time for this result (over 27 hours) is far from interactive, and therefore it is inappropriate for systems with a large or even a moderate number of components. The last column in the table above, Percent Error, is calculated for the other simulations using the power from the 348x348 simulation as a basis. The Power (at the detector) is calculated by integrating the area underneath the intensity curve. This is calculated by determining the intensity area of each grid patch and summing this value for all the grid patches in the detector plane.

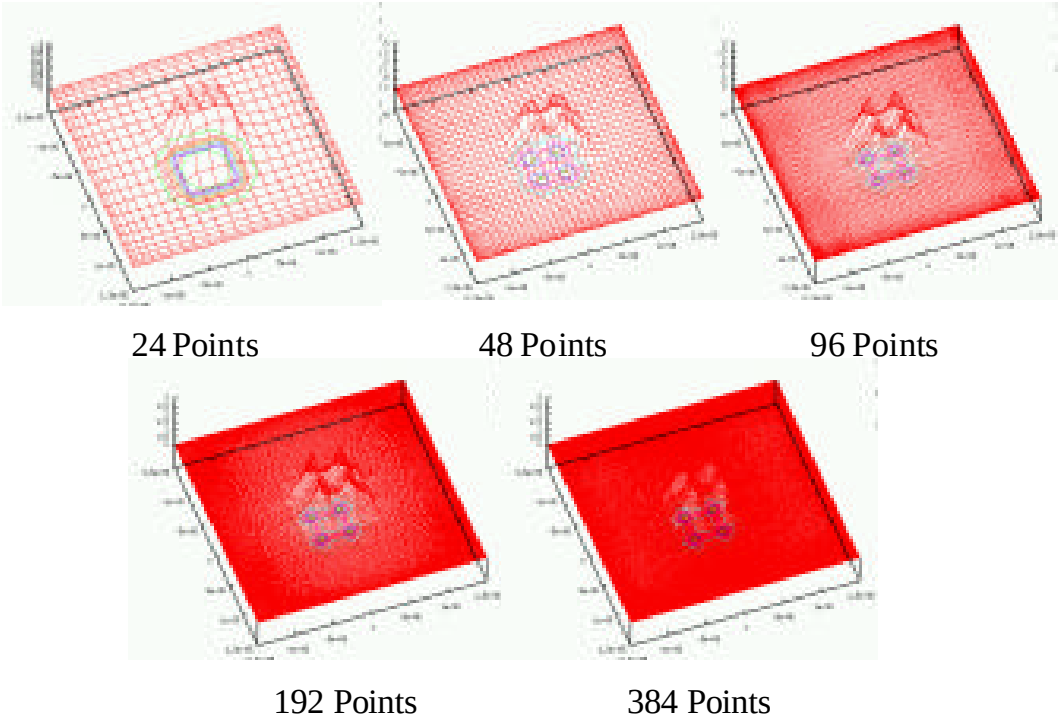

Figure 1. Intensity contours of propagation off a mirror with different number of Gaussian Quadrature mesh points.

Plotting computation time and percent error data from the simulation summary table above, we can consider an appropriate choice for the number of points that should be used in the simulation. The graph is shown in Figure 2. It appears 96x96 points for the Gaussian Quadrature method is appropriate for this simulation. No significant increase in accuracy is gained when more points are used in the integration technique. The 48x48 point case also might seem attractive since less than one percent of the accuracy is lost, and the simulation time is reduced to approximately 20 seconds. As the systems we want to simulate get larger, in terms of a greater number of optical components, reducing computation time for each surface becomes more crucial. However, any error that is generated at the first component of a multi-component optical path will be propagated throughout the remainder of the system. Therefore, in large systems, even the 0.5% of error from the 48x48 point case could be propagated through many components, each adding their own error to the wavefront, and the resulting system error could be large. It would be best if an error estimation, as well as the result, could be shown to the user at the end of the simulation as an "error bar". This is future work for our simulation framework.

It is important to note that any pre-defined mesh size is not appropriate for every simulation. It is more appropriate to talk in terms of λ/mesh length, which is also shown in the table above. Since the Gaussian Quadrature technique has uneven grid spacing, the table provides data is terms of average grid spacing, simply calculated as if the spacing was uniform. For completeness, the largest and smallest mesh sizes are given for the detector. If we consistently use this average mesh dimension notion, since in the Gaussian Quadrature method the grid size is not uniform, we can make the following observation regarding spacing, accuracy, and computation speed. To ensure accuracy, while keeping an interactive computation time, roughly 2-4 average mesh points per wavelength should be used in the simulation. Fewer mesh points than this could cause inaccuracies in the system simulation.

One could consider using a course mesh for a fast simulation, where basic system performance could be checked without the thorough examination of insertion loss, crosstalk, or error rates. By allowing the designer to choose the number of mesh points for the Gaussian Quadrature integration method, the user can trade-off accuracy and computation time in their simulations.

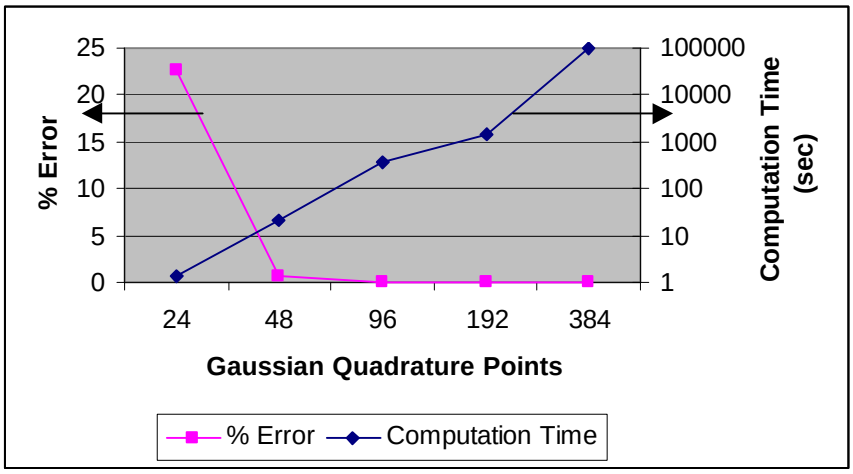

Figure 2. Graph comparing percent error and computation time for different number of Gaussian Quadrature mesh points.

2. Surface Roughness and Scattering

Scattering is a common optical effect when light strikes non-smooth surfaces. In optical MEM systems, the smoothness of the surface is determined by the material and techniques used to fabricate the component. Since we are typically interested in light reflection from a mirrored surface, in this discussion, we examine the surface roughness on an optical MEM mirror.

Commonly, surface roughness measurements are reported with a root mean square (rms) value, σ, which is defined as the standard deviation of the roughness height on the surface. In our surface modeling, we use the square of this value, σ^2, as the variance (with a mean of zero) of a normal or Gaussian distribution probability to describe the surface roughness. Therefore, for each mesh point on the surface of a component, the height (or position) of this particular section is determined by the nominal position, plus the result of calling the Gaussian distribution probability and returning a value that is defined by the particular surface roughness. This is a simple addition in the Rayleigh-Sommerfeld optical scalar formulation and for the Gaussian Quadrature method that calculates the integral. For each mesh defined by the Gaussian Quadrature technique, surface roughness is added to that value's position, resulting in a recalculation of the distance that the optical complex wavefront propagates before it strikes the component's surface.

As an example of this surface roughness modeling technique applied to a component, we simulate a plane wave striking a 10x10 μm MEM mirror and reflecting straight back towards the source. The light is detected on a 25x25 μm observation plane at a distance of 10 μm from the mirror. As seen in the previous section, the Rayleigh-Sommerfeld formulation for scalar diffractive propagation is necessary for the near field effects found in this example. Each simulation uses a Gaussian Quadrature integration technique with 96x96 mesh points. As we determined above, this allows for a good trade-off between accuracy and computation speed for this particular example system. The simulation is run five times, each time with a different surface roughness applied to the micro-mirror.

In Figure 3, intensity surface contours at the observation plane are shown from these simulations. Contour A, at the very left side of the figure, shows the result of the reflection off of a perfectly ideal smooth surface ($\sigma = 0$). The intensity distribution from this ideal simulation is given below the contour. Again, this near field shape is expected, as seen in the previous section.

Figure 3 also presents the results of the same simulation with surface roughness rms values of 10 nm, 25 nm, 50 nm, and 100 nm, shown as contours B, C, D, and E, respectively. When compared to the ideal case, (contour A), it is very noticeable how the shape of the beam deteriorates with the increase of surface roughness. As expected, with increased light scattering off of the micro-mirror, the optical power detected on the observation plane decreases with the increase of surface roughness. For each of the simulations, the amount of optical power that is lost, when compared to the ideal flat mirror, is also given in Figure 3.

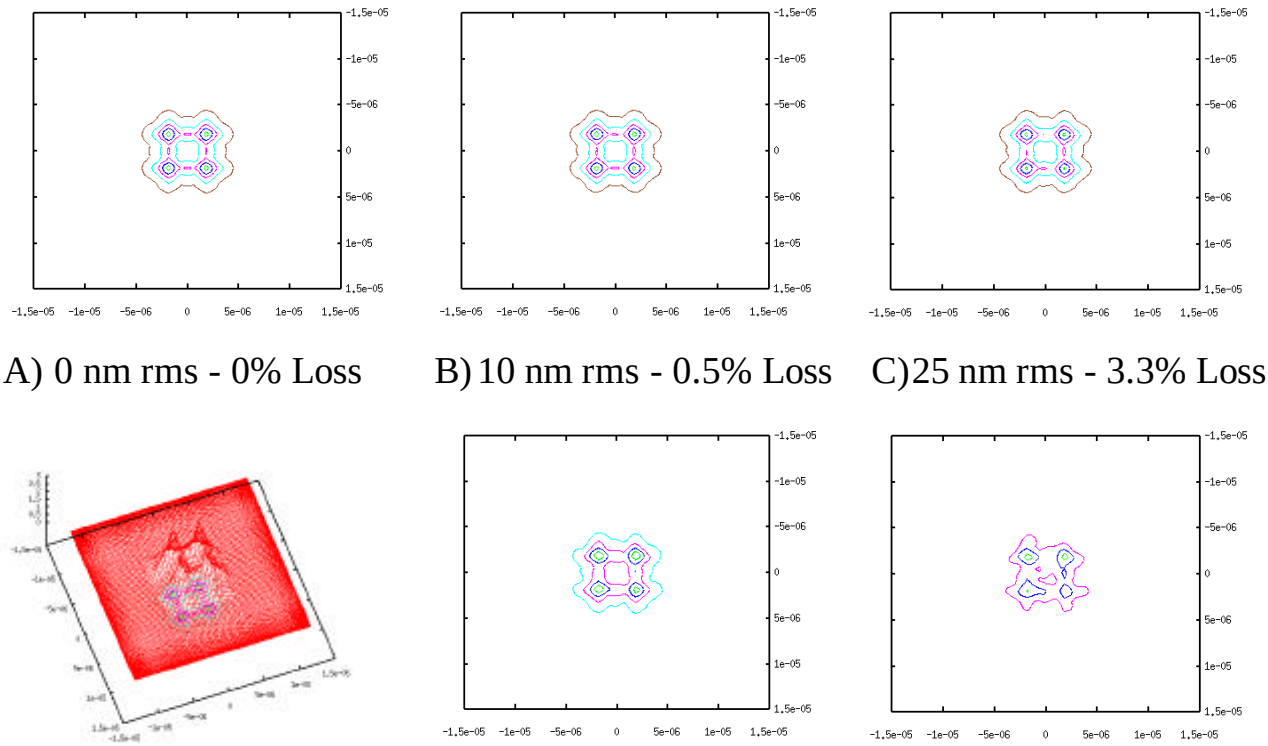

Figure 3. Intensity contours of propagation off a rough mirror.

For standard micro-mirror fabrication techniques, common values of surface roughness are fairly small. Typical surface roughnesses for thin layer deposits have peaks that range between 10 and 50 nm [4]. Therefore, the power loss from a single component due to scattering is approximately 0-10%. However, as more components are added to a system, more power can be lost resulting in an increase in system insertion loss. The scattered light also is of interest to the designer. This could lead to crosstalk in a micro-switch or back scattering, both effects that could cause a system to fail.

One can consider running simulations without a surface roughness analysis, and still approximate the power that is lost through surface roughness. A complete and detailed study could be performed of light scattering off of rough surfaces, and a generalization of the amount of optical power that is lost with a specific surface roughness could be calculated [5]. Then, probability distributions for the amount of power lost due to scattering can be pre-calculated. This allows a typical simulation to proceed, with an ideal flat mirror, and at the end of the simulation, the insertion loss analysis could use the previously calculated surface roughness loss value. Implementing this technique is future research for our modeling team. However, while the technique would work well for simple calculations of insertion loss, it would not be good for calculations of crosstalk or back scattering. For those analyses, propagating a complex wavefront of the scattered light thought the system is necessary.

3. Curvature

When fabricating micro-mirror MEM devices for an optical MEM switch, the flatness of the mirror is essential, since curvature and deformities, even more than surface roughness, can result in errors in the system. However, curved surfaces are common in optical MEM systems, since many thin components experience an inherent curvature due to factors including the fabrication material, the fabrication processes, and internal residual stress. The curvatures of these mirrors can be very large, down to a millimeter radius. Gold is commonly used as the top material of the mirror, increasing the reflectivity, however, this metal can still suffer from curvature problems [6]. As the size of the mirror increases, usually so does the curvature. Many techniques are commonly practiced in attempting to keep the mirror flat, including smaller sizes (widths and lengths) of the mechanical pieces. Another mirror-flatting fabrication technique is to create a sandwich of polysilicon-phosphosilicon-polysilicon, resulting in a mirror thickness of approximately 4 μm. This structure causes the mirror to remain

rigid, even when a metal layer (Au) is added to increase the reflectivity of the mirror. However, even with these precautions, micro-mirrors can still have serious curvature, and we need to be able to model its effects in our CAD system.

In macro-systems, spherical mirrors are often used as focusing elements and are part of the system design. In theory, this technique should also be able to be applied to optical micro-systems systems. However, due to uncontrolled variations in the fabrication process, material, and induced stresses it is impossible to consistently create the same curvature radius on every mirror on a die, wafer, or between wafers. Therefore, great effort is used to fabricate more simple flat mirrors, since optimizing a fabrication technique for flat mirrors will provide a single component that can be used in a variety of optical system designs.

The Rayleigh-Sommerfeld formulation for scalar optical propagation assumes no curvatures in either the observation or aperture plane. This is due to the general formulation not recalculating the distance of propagation for a curved surface. By examining the Rayleigh-Sommerfeld equation, we can easiest see this [7]:

$$U2(x,y) = \frac{z}{j\,l}\iint_{\Sigma} U1(x,h)\frac{\exp(jkr)}{r^2}dx\,dh \qquad r = \sqrt{z^2 + (x-x)^2 + (y-h)^2}$$

r is calculated for each point of the observation plane (x,y) with each point on the aperture plane (ξ, η). The variables used in the above equation are defined in Figure 4.

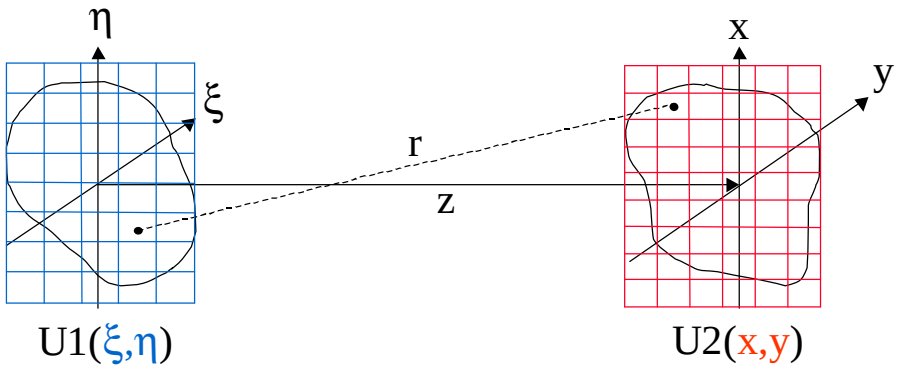

Figure 4. Diagram of the Rayleigh-Sommerfeld formulation.

Through the equation and the diagram, it is seen that the aperture and observation planes are flat, with the value of *z* being constant. However, in our use of the Gaussian Quadrature method to calculate the Rayleigh-Sommerfeld integration, we are easily able to determine the (x, y, z) center position for each mesh. This enables us to expand the Rayleigh-Sommerfeld formulation to support curvatures. Therefore, we are able to exactly calculate the distance that each wavefront travels (*r*) to get from aperture to observation plane. This allows us to model curved surfaces using an extension of the Rayleigh-Sommerfeld formulation, now using and solving three position values, with the following equation:

$$U2(x,y,z) = \frac{z}{j\,l}\iint_{\Sigma} U1(x,h,z)\frac{\exp(jkr)}{r^2}dx\,dh \qquad r = \sqrt{(z-z)^2 + (x-x)^2 + (y-h)^2}$$

We next present simulations that show the effect of using curved optical components in a micro-optical system. In these simulations, we again model reflection off of a 10x10 μm mirror, however, we now simulate a curvature (R=1mm) in the mirror. For these examples, we assume a surface roughness of zero. In Figure 5, we show intensity surface and contour distributions of light reflecting from the mirror and being detected on a 15x15 μm observation plane. The simulation result at the left of the Figure 5, (A), shows the result of reflection from an ideally flat mirror, as a basis for comparison. In the intensity distribution in the center, (B), the curvature is concave (-R), so the beam starts to converge towards the focus point of the mirror (f=R/2). In the third distribution, (C), the light strikes a convex mirror (+R), with the same degree of curvature, resulting in the divergence or spreading of the light. The simulated power detected on each of these observation planes is essentially the same, although the shape and focus (i.e., convergent or divergent) of the reflected beam is different. These effects can cause insertion loss as the beam propagates further down the optical path.

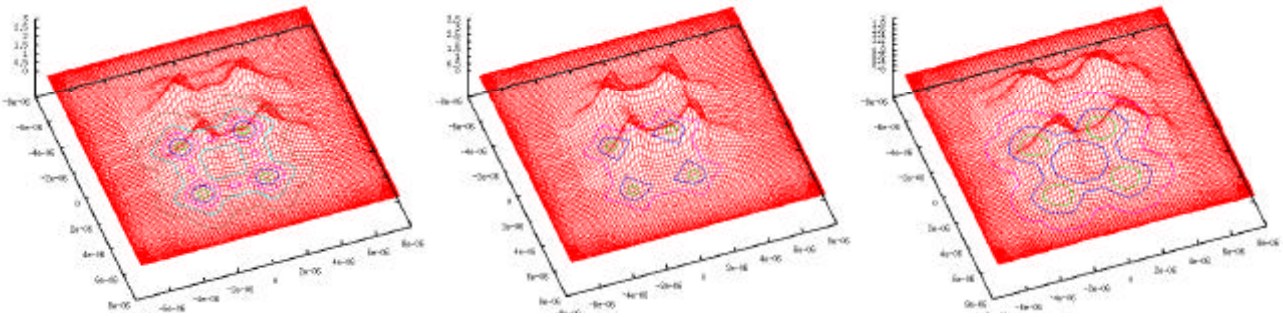

A) Flat B) Concave C) Convex

Figure 5. Intensity distributions of propagation off a curved mirror

3. MECHANICAL MODELS

We have previously reported the use of nodal analysis and piecewise linear (PWL) simulation for the modeling of mechanical structures [9]. In Chatoyant, we have implemented this methodology for the integration of mechanical elements to microsystems. In this methodology, the MEM device is modeled using a transformation of its general equation of motion into a set of first order differential equations:

$[Mb]X' + [Mk]X = [E]F$, where the state variable vector $X = \begin{bmatrix} U' \\ U \end{bmatrix}$

U is the displacement vector, and U' is the velocity vector. The expression represents a set of linear ODEs assuming the characteristic matrices are static and independent of the dynamics in the body. Each mechanical element (beam, plate, etc.) is characterized by a template composed of characteristic stiffness, damping and mass matrices. The assembly of every element into the mechanical structure is achieved by merging together their individual templates, to create the general matrix representation (*Mb*, *Mk*, *E*).

In the following section we discuss the adaptation of this technique to the simulation of curved cantilever structures.

1. Curved Cantilever Characterization

One of the more promising optical switching MEM devices is the one based on work at UCLA, shown in Figure 6 [10]. A stress-induced curved cantilever is used to move a mirror in and out of an optical path. When the mirror is in the optical path, the bar state for the switch is enable, when it is out, the switch is in the cross state.

Because of the curvature, the air gap between substrate and beam surface is progressively decreased as one moves from the mirror toward the fixed end of the structure. This fact introduces a strong electrostatic force over a section of the beam near the anchor, which in turn reduces the amount of applied voltage required to produce a specific degree of deflection on the entire structure.

A curved structure as described presents some interesting modeling challenges. Because of the electrical field applied over the length of the beam, there is an effective section of the beam making contact with the substrate (oxide insulator) as measured from the anchor reference. This contact is mechanically a "collision" between both surfaces. The contact area interface grows toward the free end and it increases as a function of the level of voltage applied. Collisions, in general, are difficult to characterize because of the necessity to quantify the interchange of energy, the momentum transformation, and the losses. An additional problem for this model is that the locations of nodes in this structure do not correspond to a simple linear arrangement. Consequently, in order to use our nodal modeling technique, the spatial location transformation for a curved structure must be defined.

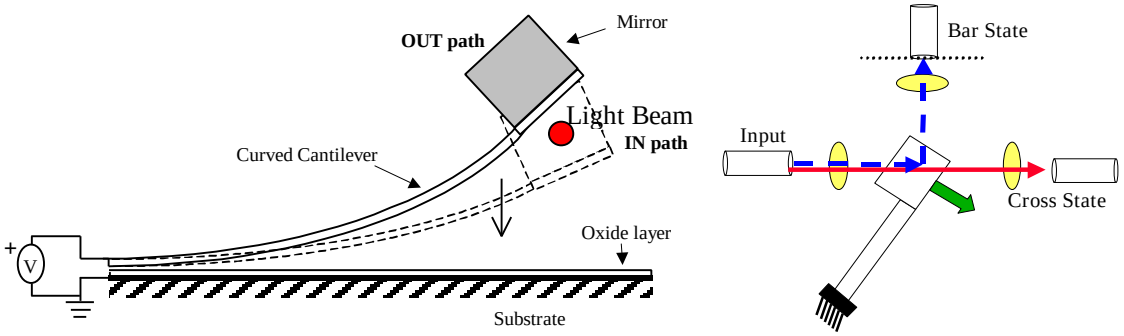

Figure 6. Stress-induced cantilever and Switching System.

2. Surface Collision:

The structure is modeled as composed of a series of basic two-node beams. This has the advantage of offering a characterization for higher modes in the structure. When an electric field is applied between the substrate and cantilever surface, all the constituting elemental beams begin to displace toward the substrate. However, the first element, measured from the fixed end, will collide with the substrate at some time before any other in the structure, as shown in Figure 7. At this time, any further linear analysis will be erroneous because of the necessity to characterize the collision. Instead of characterizing the collision we simplify the simulation by performing the simulation in discrete steps. After the collision of each section with the substrate, that section will be considered as virtually anchored to the substrate, its nodes will be unable to move. Consequently, a further characterization can be carried on as a new simulation problem where the structure is only composed of the remaining sections with initial conditions equal to the ones at an instant previous to the time of the collision. Figure 8 shows a flowchart of the described process.

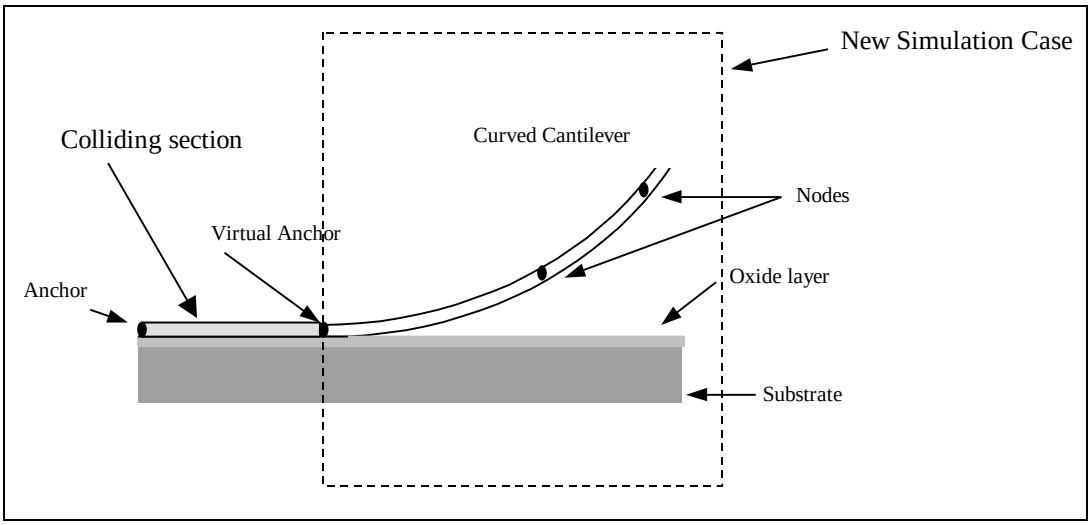

Figure 7. Step simulation in a colliding nodal characterization

3. Curvature

In our methodology, a common coordinate reference frame is used for the characterization of mechanical structures, since every template, or element, is characterized in a local reference system. The process of translation of these local templates to the global reference system can be described by [8]:

$$S = A^T \bar{S} A,$$

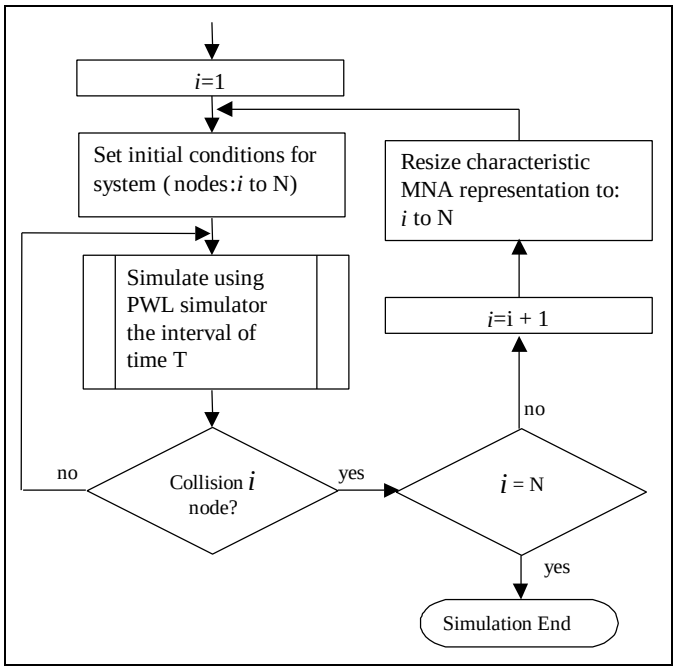

Figure 8. Piecewise Linear (PWL) discrete step simulation of a collision case

where, A represents the translation matrix from local displacements to global displacements (a function of the structure's geometry), $\overline{S}$ represents the local template, and S is the corresponding global representation.

For an element whose coordinate system is tilted in relation to the global reference system as in Figure 9 (a), the translation matrix will be according to the direction cosine of angles between the axis:

$$A = \begin{vmatrix} \cos a & \sin a & 0 & & 0 & \\ -\sin a & \cos a & 0 & & & \\ 0 & 0 & 1 & & & \\ & & & \cos a & \sin a & 0 \\ & 0 & & -\sin a & \cos a & 0 \\ & & & 0 & 0 & 1 \end{vmatrix}$$

In a curved structure composed of an assembled group of elemental beams with a constant radius of curvature r, as shown in Figure 9 (b), the individual direction cosines is proven through geometrical analysis and presented below:

$$\sin(a_i) = \frac{1}{2\sin(\frac{s}{2nr})}\left(\cos(\frac{(i-1)s}{nr}) - \cos(\frac{is}{nr})\right)$$

$$\cos(a_i) = \frac{1}{2\sin(\frac{s}{2nr})}\left(\sin(\frac{is}{nr}) - \sin(\frac{(i-1)s}{nr})\right)$$

where, n is the number of elemental beams, s is the curved length of the cantilever and i is the ith elemental beam, as seen in Figure 9 (b). With this transformation, the curved characteristic of the structure is included in the nodal characterization and simulated by the piecewise linear engine mentioned in [9]. The curved beam will be composed by a set of n two-node elemental beams of equal length ($2r\ sin(s/2nr)$). Besides the advantage of modeling a curved structure, the multi-beam characterization allows one to simulate high order modes in the simulation. As we previously suggested in [9], the technique of multi-node idealization characterizes higher order modes because of the higher number of degrees of freedom (DOF) added to the structure.

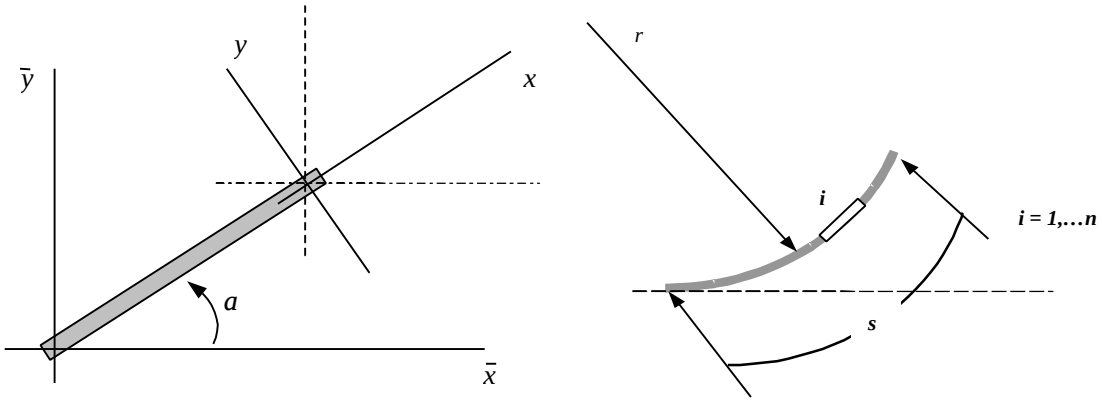

Figure 9. (a) Elemental tilted beam (b) Curved beam geometry.

4. SIMULATION

In this simulation, we perform a dynamic simulation of a 2x2 optical MEM switch. This architecture consists of a set of four optical fibers in the shape of a "+" sign, with the input and output fibers facing each other through a free-space gap. The switching system is in the "cross" state when the light is passed straight across the free-space gap. However, to switch to the "bar" state, a micro-mirror is inserted between the fibers at a 45-degree angle, and the light is reflected to the alternate output. A diagram of this system (showing only a 1x2 switching case) can be seen back in Figure 6 (b). Both the cross and bar state are shown, with solid and dashed arrows, respectively. The system as seen in the Chatoyant GUI can be seen below in Figure 10. Each icon in Chatoyant represents a component model and the path of information between them, either an optical, electrical, or mechanical signal, is represented as lines or "wires".

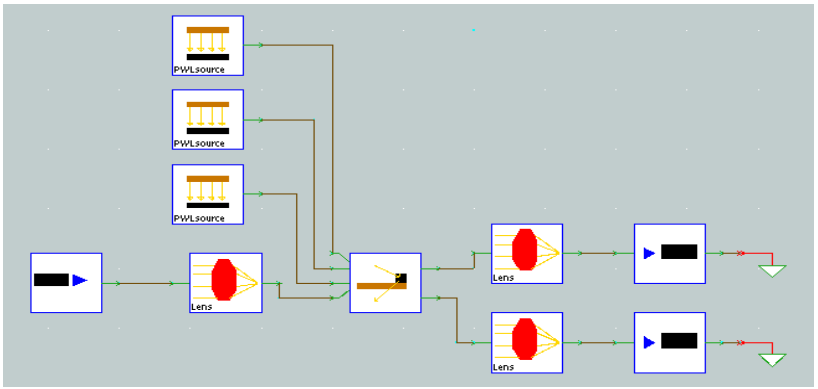

Figure 10. Chatoyant representation of 1x2 optical MEM switching system.

The optical MEM switching system that we simulate is based on a fabricated device from UCLA [10]. This 2x2 switch is based on four fibers coming to a 4-way free-space intersection. In the UCLA design, a hinged micro-mirror is fabricated at the end of an anchored mechanical beam. In the steady state, the beam is resting in the optical switching path, and the system is in the bar state. Through electrostatic attraction between the beam and the substrate of the surface, the mechanical beam can be bent towards the substrate, moving the mirror out of the optical path completing the cross state of the system.

For simplicity, we simulate only a single input switching to either the cross or bar state throughout this example. The mirror is 100 x 100 μm, and is positioned at the end of a 700 μm cantilever beam. Both beam and mirror are fabricated with polysilicon, with the mirror having an ideal reflectivity of 100%. The beam is 2 μm thick and 100 μm wide, while the mirror is 4 μm thick, to counteract the induced residual stress that otherwise would curve the mirror. Collimating lenses (f = 50 μm) are placed 50 μm from the fiber ends, and there is a free-space gap of 100 μm between the lenses. The mirror, when placed in the optical path, is positioned in the center of the free-space gap, 50 μm from each lens.

The modeling of the mechanical beam and electrostatic attraction is performed using the PWL technique described above. Chatoyant's optical modeling technique is also based on the work introduced above. RSoft's BeamPROP [11] is used to simulate the light through the fiber, as we have developed an interface between the fiber propagation (BeamPROP) and free-space (Chatoyant) through a data file.

We first examine the simulation of the switch with an input force rise and fall time of 600 μsec, caused by electrostatic attraction between the cantilever beam and the substrate. The response of this optical power detected on the bar state of the fiber is shown in Figure 11 (A). A concern of this system is the response of the cantilever beam, as it moves from one state to the other. In this case of a long enough switching time, the optical power follows in both the bar and cross state, with respect to following the input electrostatic force. However, when the switching time is decreased, the beam's response to the electrostatic force can "bounce" the mirror back into the optical path. This is because the faster switching input energizes fundamental modes in the cantilever beam, which respond with damped oscillations at the fundamental mode frequencies. Therefore, even though the switch is in the specified state, the other state might receive some power, as the mirror "bounces" due to the response of the cantilever beam to the electrostatic attraction. The effect can cause crosstalk, or worse yet, achieve an error in the signal. This effect can be seen in Figure 11 (B), as the rise and fall time are decreased to 400 μsec. Notice that the response of the beam causes power to be detected on the bar state, even though the bar state should detect zero power. This can be seen, in the small peaks at 600, 850, 1100 μsec. As expected, as the response of the beam settles to the steady state, less power is captured each time the mirror bounces into the optical path, evident that the 600 μsec peak power is larger than the 1100 μsec peak power. In each of the simulations, the input switching force (with respect only to the x axis, time) is represented by the dashed line.

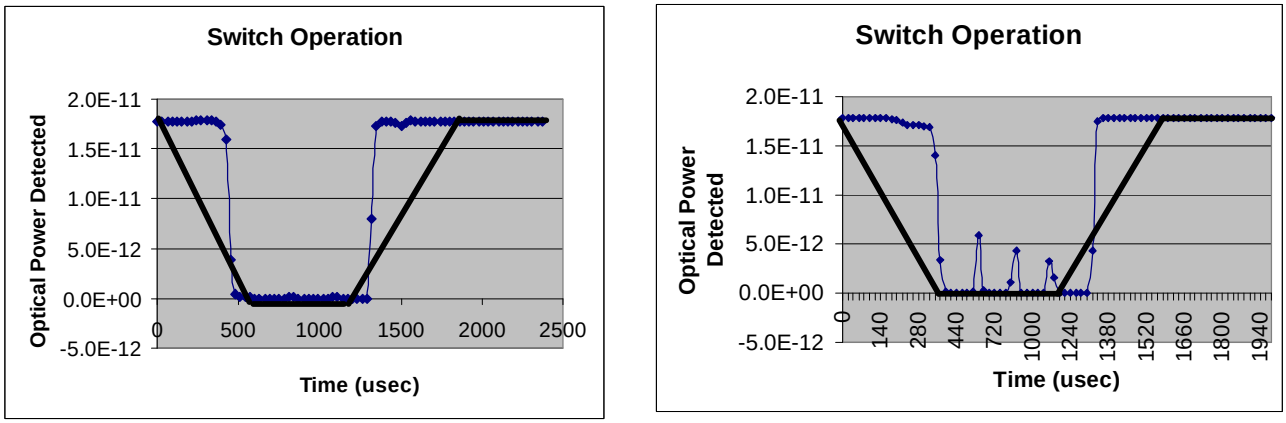

Figure 11. Power output detected on bar fiber for switching times of (A) 600 and (B) 400 μsec.

5. CONCLUSIONS

With the advancement of models in our Chatoyant framework, simulations are accurate and realistic, helping the design of optical MEM systems. The systems simulated can be composed of non-ideal components allowing the CAD tool to catch the unexpected design flaws. CAD tools are most advantageous and useful when they can notify a designer of errors before the costly fabrication and testing stage of design. With realistic component models, these unexpected errors can be found in system-level simulations and redesigned so the prototyping of the system has a high probability of success in the first fabrication run.

6. ACKNOWLEDGEMENTS

We would like to acknowledge the support of NSF grants ECS-9616879 and CCR-9988319.

7. REFERENCES

1. T.P. Kurzweg, S.P. Levitan, P.J. Marchand, J.A. Martinez, K.R. Prough, D.M. Chiarulli, "CAD for Optical MEMS," *Proceedings of the 36th IEEE/ACM Design Automation Conference (DAC'99)*, New Orleans, LA, June 20-25, 1999, pp. 879-884.
2. T.P. Kurzweg, S.P. Levitan, J.A. Martinez, P.J. Marchand, D.M. Chiarulli, "Diffractive Optical Propagation Techniques for a Mixed-Signal CAD Tool," *Optics in Computing (OC2000)*, Quebec City, CA, June 18-23, 2000.

3. A.H. Stroud, D. Secrest, *Gaussian Quadrature Formulas*, Englewood Cliffs, N.J., Prentice-Hall, 1966.
4. M. Beggans, K. Farmer, J. Federici, T.G. Digges, Jr., S. Garofalini, D. Hensley, "Bondability and Surface Roughness of Ultra-Thin Single Crystal Silicon Wafers," *International Symposium of Semiconductor Wafer Bonding*, Proceedings Volume 97-36, Pennington, NJ, 1997.
5. C. Marxer, M.-A. Gretillat, N.F. de Rooij, R. Battig, O. Anthamatten, B. Valk, P. Vogel, "Vertical Mirrors Fabricated by Reactive Ion Etching for Fiber Optical Switching Applications," *MEMS 1997*, 1997, pp. 49-54.
6. M.C. Wu, "Micromachining for optical and Optoelectronic Systems," *Proceedings of the IEEE*, Vol. 85, No. 11, November 1997, pp. 1833-1856.
7. J.W. Goodman, *Introduction to Fourier Optics*, Second Edition (The McGraw-Hill Companies, Inc., 1996).
8. J.S. Przemieniecki, *Theory of Matrix Structural Analysis*, (McGraw-Hill, New York, New York, 1968).
9. S.P. Levitan, J.A. Martinez, T.P. Kurzweg, P.J. Marchand, D.M. Chiarulli, "Mixed-Technology System-Level Simulation," *Design, Test, Integration, and Packaging of MEMS/MOEMS*, Paris, France, May 9 - 11, 2000.
10. R.T. Chen, H. Nguyen, M.C. Wu, "A High-Speed Low-Voltage Stress-Induced Micromachined 2x2 Optical Switch," *IEEE Photonics Technology Letters*, Vol.11, No. 11, Nov. 1999, pp.1396-1398.
11. Rsoft, Inc., http://www.rsoftinc.com/.